Pressure-driven radial flow in a Taylor–Couette cell

NILS TILTON[1], DENIS MARTINAND[1]†, ERIC SERRE[1] AND RICHARD M. LUEPTOW[2]

[1]Laboratoire M2P2, UMR 6181, Université Aix-Marseille, CNRS, 13451 Marseille, France

[2]Department of Mechanical Engineering, Northwestern University, Evanston, IL 60208 USA

A generalized solution for pressure-driven flow through a permeable rotating inner cylinder in an impermeable concentric outer cylinder, a situation used commercially in rotating filtration, is challenging due to the interdependence between the pressure drop in the axial direction and that across the permeable inner cylinder. Most previous approaches required either an imposed radial velocity at the inner cylinder or radial throughflow with both the inner and outer cylinders being permeable. We provide an analytical solution for rotating Couette–Poiseuille flow with Darcy's law at the inner cylinder by using a small parameter related to the permeability of the inner cylinder. The theory works for suction, injection and even combined suction/injection, when the axial pressure drop in the annulus is such that the transmembrane pressure difference reverses sign along the axial extent of the system. Corresponding numerical simulations for finite-length systems match the theory very well.

---

1. Introduction

One practical application of Taylor–Couette flow is rotating filtration. In these systems, a permeable inner cylinder rotates in an impermeable concentric outer cylinder. As a feed suspension or solution is pumped axially through the annulus between the cylinders, a purified filtrate is extracted through the permeable cylinder. Rotating filtration reduces the undesirable build up of solutes or particles adjacent to the membrane because the shear due to the rotating cylinder and the vortical structures that develop in the annulus wash contaminants away from the inner cylinder. Rotating filtration has been demonstrated experimentally for a wide range of permeabilities and solutions (Jaffrin 2008), and also has applications for mixing and emulsification. Though the subject of more than 30 papers since 1990, the fluid mechanics of rotating filtration are not completely understood. The complex fluid flow in the device includes transmembrane flow with a varying transmembrane pressure difference, the transport of particles or solutes and the appearance of Taylor vortices. Here we address the issue of laminar Couette–Poiseuille flow before the appearance of vortices, with a pressure-dependent boundary condition for the transmembrane flow. An analytical solution for this flow under realistic conditions has not been available to date. This has hindered the study of near-membrane transport phenomena related

† Email address for correspondence: denis.martinand@L3M.univ-mrs.fr

to the coupling between the transmembrane pressure and flow, such as cake layers, concentration boundary layers, osmotic pressure and membrane fouling, as well as large-scale phenomena such as the effects of the axial inhomogeneity of the base flow on global stability and the transport of particles or solutes.

Even relatively simple flows with suction or injection through permeable walls have proved challenging. Early studies of channels (Berman 1953), cylindrical pipes (Yuan & Finkelstein 1956) and annuli (Berman 1958; Morel, Lavan & Bernstein 1977) prescribed a uniform wall-normal velocity at the permeable surface. In real applications, however, the wall-normal velocity generally depends on the pressure at the wall. A pressure-dependent approach was first used by Taylor (1956) for flow through porous tubes and cones. Subsequently, several studies have considered a pressure-dependent approach based on Darcy's law for simple symmetric geometries such as channel flows with two equally permeable walls (Haldenwang 2007) or porous tubes (Regirer 1960; Galowin, Fletcher & DeSantis 1974; Damak *et al.* 2004). Previous studies related to rotating filtration focus primarily on centrifugal instability. In these cases, the simpler problem of a Couette–Poiseuille flow with an imposed radial flow through two permeable cylinders is considered because there exists an axially independent analytical solution amenable to modal linear stability analysis (see Martinand, Serre & Lueptow 2009, and references therein). Analytical solutions for cases with a single permeable cylinder are also available, but they prescribe a constant wall-normal velocity at the permeable wall, and assume that the radial velocity field is independent of the axial direction (Belfort *et al.* 1993; Marques, Sanchez & Weidman 1998), neither of which is generally true in a rotating filter.

This study presents a formulation for Couette–Poiseuille flow with Darcy's law at the permeable rotating inner cylinder while constraining the outer cylinder to be impermeable, thus matching the conditions for rotating filtration systems. The approach works for radial suction or injection, and the pressure and velocity fields generally depend slowly on the axial position. This makes possible the analysis of a situation known as crossflow reversal, where flow through the permeable cylinder reverses from suction to injection due to the axial pressure drop, as well as a situation known as axial flow exhaustion, where axial flow is exhausted due to suction through the permeable wall. Both situations are important because they are typically undesirable in industrial applications. The analytical solution shows excellent agreement with corresponding numerical simulations for finite-length systems.

2. Presentation of problem and analytical solution

We consider the steady incompressible axisymmetric Couette–Poiseuille flow illustrated in figure 1. An annular fluid region is delimited by two concentric cylinders of infinite axial extent of radii R_1 and R_2, where $R_1 < R_2$. The outer cylinder is stationary and impermeable. The inner cylinder is made of a thin permeable membrane of thickness h which rotates about its longitudinal axis with constant angular velocity Ω. We assume that a cylindrical fluid cavity, $0 \leqslant r \leqslant R_1 - h$, in the porous cylinder is maintained at a constant uniform pressure P_{ref}. The rotating inner cylinder drives an azimuthal Couette flow, v, while an axial pressure gradient drives an axial annular Poiseuille flow, w. The transmembrane pressure difference between the annulus and cavity results in a radial suction or injection, u, which varies with z.

The flow is governed by the steady Navier–Stokes and continuity equations. On the outer cylinder, we apply the conditions $u = v = w = 0$. On the permeable inner cylinder, we assume that v and w satisfy the no-slip condition, while u is related to
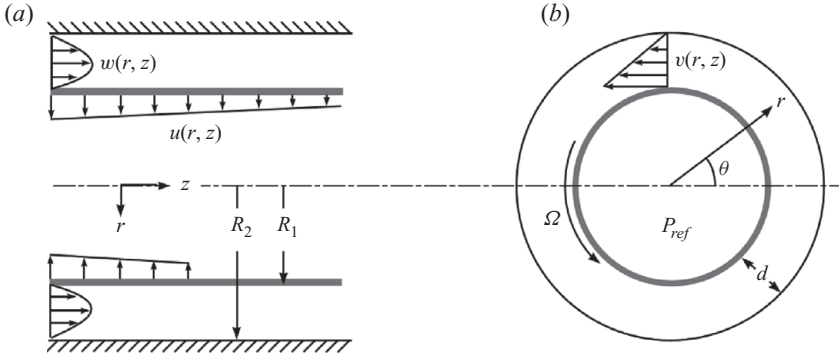
FIGURE 1. Sketch of the annular geometry and laminar velocity profile, not to scale, considered in this study: (*a*) r–z plane, (*b*) r–θ plane.

the transmembrane pressure difference through Darcy's law,

$$u = -\frac{k}{\mu h}(p|_{r=R_1} - P_{ref}), \qquad v = \Omega R_1, \qquad w = 0, \qquad (2.1)$$

where p and μ are the fluid pressure and dynamic viscosity, respectively, and k is the membrane permeability and has the units length squared. Without loss of generality, we set $P_{ref} = 0$. Guided by typical inlet conditions for a laboratory experiment, we prescribe the transmembrane pressure difference P_{tm} and mean axial flow rate $\overline{W}$ at $z = 0$,

$$P_{tm} = p|_{r=R_1, z=0}, \qquad \overline{W} = \frac{1}{\pi(R_2^2 - R_1^2)} \int_{R_1}^{R_2} w|_{z=0} 2\pi r \, dr. \qquad (2.2)$$

Note that prescribing P is equivalent to prescribing the transmembrane velocity at the inlet, $U_{tm} = u(R_1, 0) = -kP_{tm}/(\mu h)$.

Generally, flows over permeable surfaces may have a non-zero tangential velocity at the surface due to momentum transfer from the fluid region to the fluid in the porous material (Beavers & Joseph 1967). The no-slip assumption is reasonable, however, when a permeable surface is made up of small discrete holes, such that the permeability is zero in the tangential directions, and the percentage area of the pores on the permeable surface is small. In this case, the fluid flow is mostly normal to the surface and the tangential velocity in the pores may be neglected.

We seek a solution to our problem in the form of an asymptotic expansion when variations in the axial direction are small compared to those in the radial direction. To motivate our approach, we introduce the following characteristic scales:

$$u \sim U_{tm}, \quad w \sim \overline{W}, \quad v \sim \Omega R_1, \quad p \sim P_{tm}, \quad r \sim d, \quad z \sim L. \qquad (2.3)$$

We assume that variations in the radial direction scale with the annulus width $d = R_2 - R_1$, while those in the axial direction scale with L, which remains to be defined. Note that studies of Couette flow often scale the pressure with $\rho \Omega^2 R_1^2$, where ρ is the fluid density. In (2.3), however, we use P_{tm} to stress the relationship between the transmembrane velocity and pressure. Though either pressure scale can be used, P_{tm} leads to the simplest definition of L. To illustrate one potential choice for L, consider the particular case of flow between two impermeable cylinders, i.e. $k = 0$. In this case, the pressure varies over an axial length scale L_p such that the pressure term balances the viscous term in the axial momentum equation, $\partial_z p = \mu(\partial_r^2 w + r^{-1}\partial_r w)$.

Using relations (2.3) it can be then shown that d/L_p scales like

$$\frac{d}{L_p} \sim \frac{\mu \overline{W}}{d P_{tm}}. \tag{2.4}$$

To illustrate another potential choice for L, consider the dead-end length, L_{de}, where the axial flow is completely exhausted due to transmembrane suction. If the suction velocity is constant over the entire cylinder, it can be shown that

$$\frac{d}{L_{de}} \sim \frac{2}{1+\eta} \frac{|U_{tm}|}{\overline{W}} = \frac{2}{1+\eta} \frac{d P_{tm}}{\mu \overline{W}} \sigma, \tag{2.5}$$

where $\sigma = k/(hd)$ is the non-dimensional permeability and $\eta = R_1/R_2$. Note that $2/(1+\eta)$ is of order one.

Variations in the axial direction are small compared to those in the radial direction when the ratios d/L_p and d/L_{de} are both of order ϵ, where $\epsilon \ll 1$ is a small parameter. From (2.4)–(2.5), it follows that

$$\frac{d^2}{L_p L_{de}} \sim \sigma = O(\epsilon^2). \tag{2.6}$$

Motivated by (2.6), we define $\epsilon = \sqrt{\sigma}$ and $L = d/\epsilon$. Because σ typically varies between 10^{-10} and 10^{-8} (see Jaffrin 2008), $\epsilon = \sqrt{\sigma}$ is a physically natural parameter about which to attempt an asymptotic expansion.

We introduce the non-dimensionalized variables

$$\hat{\boldsymbol{v}} = \frac{\boldsymbol{v}}{\Omega R_1}, \qquad \hat{p} = \frac{p}{\rho \Omega^2 R_1^2}, \qquad \hat{r} = \frac{r}{d}, \qquad \hat{Z} = \frac{z}{L} = \epsilon \frac{z}{d}, \tag{2.7}$$

where $\boldsymbol{v} = [u \ v \ w]^{\mathrm{T}}$. Note that the length scales for $\hat{r}$ and $\hat{Z}$ differ by a factor ϵ. To be consistent with the existing literature, $\hat{\boldsymbol{v}}$ and $\hat{p}$ are made non-dimensional using ΩR_1 and $\rho \Omega^2 R_1^2$, respectively. We define the rotational Reynolds number as $Re = \rho \Omega R_1 d/\mu$. All subsequent equations and parameters are non-dimensional. For notational convenience, we omit the $\hat{\ }$ symbol from the non-dimensional variables. The governing equations and boundary conditions are

$$u\partial_r u - r^{-1}v^2 + \epsilon w\partial_Z u + \partial_r p - Re^{-1}\left(\partial_r^2 u + r^{-1}\partial_r u - r^{-2}u + \epsilon^2\partial_Z^2 u\right) = 0, \tag{2.8a}$$

$$u\partial_r v + r^{-1}uv + \epsilon w\partial_Z v - Re^{-1}\left(\partial_r^2 v + r^{-1}\partial_r v - r^{-2}v + \epsilon^2\partial_Z^2 v\right) = 0, \tag{2.8b}$$

$$u\partial_r w + \epsilon w\partial_Z w + \epsilon\partial_Z p - Re^{-1}\left(\partial_r^2 w + r^{-1}\partial_r w + \epsilon^2\partial_Z^2 w\right) = 0, \tag{2.8c}$$

$$\partial_r u + r^{-1}u + \epsilon\partial_Z w = 0, \tag{2.8d}$$

$$u = -\epsilon^2 Re\, p, \quad v = 1, \quad w = 0, \quad \text{on} \quad r = R_1, \tag{2.8e}$$

$$u = v = w = 0, \quad \text{on} \quad r = R_2, \tag{2.8f}$$

$$p|_{r=R_1} = P_{tm}, \quad \overline{w} = \overline{W}, \quad \text{on} \quad z = 0, \tag{2.8g}$$

where $\partial_r = \partial/\partial r$ and $\partial_Z = \partial/\partial Z$. Consistent with (2.7), the quantities $R_1 = \eta/(1-\eta)$, $R_2 = 1/(1-\eta)$, P_{tm} and $\overline{W}$ are all non-dimensional. Darcy's law appears in (2.8e) through the relation $\sigma = k/hd = \epsilon^2$. We seek a solution in the form of the following asymptotic expansion:

$$(\boldsymbol{v}, p) = (\boldsymbol{v}_0, p_0) + \epsilon(\boldsymbol{v}_1, p_1) + \epsilon^2(\boldsymbol{v}_2, p_2) + O(\epsilon^3). \tag{2.9}$$

Substituting (2.9) into (2.8) and sorting by powers of ϵ, yields an hierarchy of systems of partial differential equations and boundary conditions.

2.1. *The zero-order problem*

The governing equations and boundary conditions for the zero-order problem are

$$u_0 \partial_r u_0 - r^{-1} v_0^2 + \partial_r p_0 - Re^{-1} \left(\partial_r^2 u_0 + r^{-1} \partial_r u_0 - r^2 u_0 \right) = 0, \tag{2.10a}$$

$$u_0 \partial_r v_0 + r^{-1} u_0 v_0 - Re^{-1} \left(\partial_r^2 v_0 + r^{-1} \partial_r v_0 - r^{-2} v_0 \right) = 0, \tag{2.10b}$$

$$u_0 \partial_r w_0 - Re^{-1} \left(\partial_r^2 w_0 + r^{-1} \partial_r w_0 \right) = 0, \tag{2.10c}$$

$$\partial_r u_0 + r^{-1} u_0 = 0. \tag{2.10d}$$

$$u_0 = w_0 = 0, \quad v_0 = 1, \quad \text{on} \quad r = R_1, \tag{2.10e}$$

$$u_0 = v_0 = w_0 = 0, \quad \text{on} \quad r = R_2. \tag{2.10f}$$

Equations (2.10a)–(2.10f) are readily solved to show that

$$u_0 = w_0 = 0, \quad v_0 = \frac{R_1 \left(R_2^2 - r^2 \right)}{Ar}, \quad p_0 = \frac{R_1^2 R_2^2}{2A^2} \left(\frac{r^2}{R_2^2} - \frac{R_2^2}{r^2} - 4 \ln r \right) + p_0^Z(Z), \tag{2.11}$$

where $A = R_2^2 - R_1^2$ and p_0^Z is an unknown function of Z. The zero-order solution is a cylindrical Couette flow with the addition of an unknown Z-dependence in the pressure.

2.2. *The first-order problem*

The governing equations and boundary conditions for the first-order problem are

$$-2r^{-1} v_0 v_1 + \partial_r p_1 - Re^{-1} \left(\partial_r^2 u_1 + r^{-1} \partial_r u_1 - r^{-2} u_1 \right) = 0, \tag{2.12a}$$

$$u_1 \partial_r v_0 + r^{-1} v_0 u_1 - Re^{-1} \left(\partial_r^2 v_1 + r^{-1} \partial_r v_1 - r^{-2} v_1 \right) = 0, \tag{2.12b}$$

$$\partial_Z p_0 - Re^{-1} \left(\partial_r^2 w_1 + r^{-1} \partial_r w_1 \right) = 0, \tag{2.12c}$$

$$\partial_r u_1 + r^{-1} u_1 = 0. \tag{2.12d}$$

$$u_1 = v_1 = w_1 = 0, \quad \text{on} \quad r = R_1 \quad \text{and} \quad R_2. \tag{2.12e}$$

From (2.12a), (2.12b) and (2.12d), we find that u_1, v_1 and $\partial p_1/\partial r$ are all zero. Next, we solve (2.12c) using separation of variables, $w_1 = w_1^r(r) w_1^Z(Z)$, and find that

$$w_1^Z = -Re \frac{\mathrm{d} p_0^Z}{\mathrm{d} Z}, \quad w_1^r = \frac{A \ln r + (\ln \eta) r^2 + B}{-4 \ln \eta}, \tag{2.13}$$

where $B = R_1^2 \ln R_2 - R_2^2 \ln R_1$. Solution (2.13) is similar to annular Poiseuille flow with the exception that $\mathrm{d} p_0^Z/\mathrm{d} Z$ and consequently w_1 may vary with Z.

2.3. *The second-order problem*

The governing equations and boundary conditions for the second-order problem are

$$-2r^{-1} v_0 v_2 + \partial_r p_2 - Re^{-1} \left(\partial_r^2 u_2 + r^{-1} \partial_r u_2 - r^{-2} u_2 \right) = 0, \tag{2.14a}$$

$$u_2 \partial_r v_0 + r^{-1} u_2 v_0 - Re^{-1} \left(\partial_r^2 v_2 + r^{-1} \partial_r v_2 - r^{-2} v_2 \right) = 0, \tag{2.14b}$$

$$\partial_Z p_1 - Re^{-1} \left(\partial_r^2 w_2 + r^{-1} \partial_r w_2 \right) = 0, \tag{2.14c}$$

$$\partial_r u_2 + r^{-1} u_2 + \partial_Z w_1 = 0. \qquad (2.14d)$$

$$v_2 = w_2 = 0, \quad u_2 = -Re\, p_0, \quad \text{on} \quad r = R_1, \qquad (2.14e)$$

$$u_2 = v_2 = w_2 = 0, \quad \text{on} \quad r = R_2. \qquad (2.14f)$$

The boundary conditions at second-order are similar to those for the first-order problem with the exception that Darcy's law appears at the inner cylinder. To solve the second-order problem, we seek a solution to u_2 using separation of variables as expected from (2.13), $u_2 = u_2^r(r) u_2^Z(Z)$, and solve (2.14d) with the condition $u_2 = 0$ at $r = R_2$,

$$u_2^Z = -Re \frac{\mathrm{d}^2 p_0^Z}{\mathrm{d}Z^2}, \quad u_2^r = \frac{1}{16 \ln \eta} \left[\frac{C}{r} + 2Ar \ln r + (2B - A)r + (\ln \eta) r^3 \right], \qquad (2.15)$$

where $C = A R_2^2 + R_2^4 \ln \eta$. Substituting (2.11) and (2.15) into the Darcy condition in (2.14e) produces an ordinary differential equation which we solve for p_0^Z,

$$p_0^Z = M \mathrm{e}^{Z/\lambda} + N \mathrm{e}^{-Z/\lambda} - D, \quad D = \frac{R_1^2 R_2^2}{2A^2}(\eta^2 + \eta^{-2} - 4 \ln R_1), \quad \lambda = \sqrt{u_2^r(R_1)}, \quad (2.16)$$

where M and N are constants determined by prescribing two independent quantities among p_0, w_1 or u_2 at two arbitrary, possibly coincident, axial locations. Applying conditions (2.8g) yields

$$M = \frac{P_{tm}}{2} - \frac{\lambda \overline{W}}{2\epsilon Re\, \overline{w_1^r}}, \quad N = \frac{P_{tm}}{2} + \frac{\lambda \overline{W}}{2\epsilon Re\, \overline{w_1^r}}, \quad \text{with} \quad \overline{w_1^r} = \frac{(R_1^2 + R_2^2) \ln \eta + A}{8 \ln \eta}, \quad (2.17)$$

where $\overline{w_1^r}$ is the mean of w_1^r defined in an analogous manner as $\overline{W}$ in (2.2). We solve (2.14b) using separation of variables, $v_2 = v_2^r(r) v_2^Z(Z)$, and find that $v_2^Z = Re^2(\mathrm{d}^2 p_0^Z/\mathrm{d}Z^2)$,

$$\left. \begin{aligned} v_2^r &= \frac{R_1}{128 A \ln \eta} \left[Er + \frac{F}{r} + 8Cr \ln r + 4Ar^3 \ln r + (4B - 5A)r^3 + \frac{2}{3}(\ln \eta) r^5 \right], \\ E &= -8 \frac{C}{A} \left(R_2^2 \ln R_2 - R_1^2 \ln R_1 \right) + \frac{10 \ln \eta}{3} \left(R_1^4 + R_1^2 R_2^2 + R_2^4 \right) + 5 \left(R_2^4 - R_1^4 \right), \\ F &= -R_1^2 R_2^2 \left[8 \frac{C}{A} \ln \eta + \frac{10 \ln \eta}{3} \left(R_1^2 + R_2^2 \right) + 5A \right]. \end{aligned} \right\} \quad (2.18)$$

The solution for w_2 and p_1 requires that we solve the third-order problem resulting in $w_2 = p_1 = 0$. To solve (2.14a) for p_2 requires solving the fourth-order problem. For brevity, we do not report the result because p_2 has no effect on v_2. Moreover, in §3 we illustrate that p_0 already shows an excellent agreement with numerical simulation.

3. Results and discussion

The resulting analytical solution may be written as

$$u(r, z) = \epsilon^2 u_2 = -u_2^r \left[\sigma \frac{Re\, P_{tm}}{\lambda^2} \cosh(\zeta) - \sqrt{\sigma} \frac{\overline{W}}{\lambda \overline{w_1^r}} \sinh(\zeta) \right], \qquad (3.1a)$$

$$v(r, z) = v_0 + \epsilon^2 v_2 = \frac{R_1 \left(R_2^2 - r^2 \right)}{Ar} + v_2^r \left[\sigma \frac{Re^2 P_{tm}}{\lambda^2} \cosh(\zeta) - \sqrt{\sigma} \frac{Re\, \overline{W}}{\lambda \overline{w_1^r}} \sinh(\zeta) \right], \qquad (3.1b)$$

$$w(r, z) = \epsilon w_1 = w_1^r \left[\frac{\overline{W}}{w_1^r} \cosh(\zeta) - \sqrt{\sigma} \frac{Re\, P_{tm}}{\lambda} \sinh(\zeta) \right], \quad (3.1c)$$

$$p(r, z) = p_0 = \frac{R_1^2 R_2^2}{2A^2} \left(\frac{r^2}{R_2^2} - \frac{R_2^2}{r^2} - 4\ln r \right) + P_{tm} \cosh(\zeta) - \frac{\lambda \overline{W}}{\sqrt{\sigma} Re\, w_1^r} \sinh(\zeta) - D, \quad (3.1d)$$

where $\zeta = z\sqrt{\sigma}/\lambda$, with z non-dimensionalized with respect to d, i.e. $z = ZL/d = Z/\epsilon$. Solution (3.1) has several interesting limiting cases. As $\eta = R_1/R_2$ approaches unity, (3.1) tends to a planar Couette–Poiseuille flow with pressure-dependent suction at one wall. As η tends to zero, the inner cylinder tends to the superposition of a line vortex and pressure-dependent sink. In the limit $\sigma \to 0$, it can be shown using l'Hopital's rule that (3.1) recovers the classical solution for Couette–Poiseuille flow in an annulus.

For finite permeabilities, solution (3.1) predicts the conditions for which crossflow reversal (CFR) or axial flow exhaustion (AFE) occur. CFR, in which the transmembrane flow changes from suction to injection, occurs at z_{CFR} where $u(R_1, z_{CFR}) = 0$. AFE, in which the axial flow reverses and fluid is drawn from both ends of the annulus, occurs at z_{AFE} where the mean axial flow rate vanishes, $\overline{w}(z_{AFE}) = 0$. From (3.1), we find that

$$z_{CFR} = \frac{\lambda}{\sqrt{\sigma}} \tanh^{-1}(1/\beta), \quad z_{AFE} = \frac{\lambda}{\sqrt{\sigma}} \tanh^{-1}\beta, \quad \text{with} \quad \beta = \frac{\overline{W}\lambda}{\sqrt{\sigma} Re\, P_{tm}\, \overline{w_1^r}}. \quad (3.2)$$

CFR occurs when $|\beta| > 1$, while AFE occurs when $|\beta| < 1$. Both z_{CFR} and z_{AFE} tend to infinity as $|\beta| \to 1$. When $|\beta| \neq 1$, (3.1) predicts exponential behaviour as $z \to \pm\infty$ due to the $\cosh(\zeta)$ and $\sinh(\zeta)$ terms. For the marginal cases $\beta = \pm 1$, however, (3.1) predicts that the balance between the transmembrane and axial flows is such that $\partial p/\partial z$, w and u tend to zero in the limit $z \to \infty$ for $\beta = 1$, and $z \to -\infty$ for $\beta = -1$. These limiting cases tend to a classical Couette flow despite the non-zero permeability. For a rotating filtration system with a given σ, η, Ta and finite axial length, (3.2) predicts which combinations of $\overline{W}$ and P_{tm} are necessary to avoid CFR and AFE, respectively.

Available experimental studies use solutions or suspensions as working fluids and consider supercritical flow regimes exhibiting vortical structures (see Jaffrin 2008, for a partial review). We, therefore, validate (3.1) by performing a comparison with direct numerical simulations of the unsteady axisymmetric Navier–Stokes and continuity equations in a system with a radius ratio, $\eta = 0.85$, and finite axial length, $-30 \leqslant z \leqslant 30$, typical of values for experiments (see, for example Min & Lueptow 1994). For this purpose, we modify the Chebyshev–Chebyshev pseudo-spectral method of Serre & Pulicani (2001) to accommodate Darcy's law at $r = R_1$. To avoid computational difficulties related to the boundary conditions at the ends of the porous region, we introduce buffer regions near the inlet, $-30 \leqslant z \leqslant -20$, and outlet, $20 \leqslant z \leqslant 30$, where we multiply the permeability by a function $b(z)$ which tends smoothly to zero at $z = \pm 30$. At the inlet, $z = -30$, a classical Couette–Poiseuille flow ($\sigma = 0$) with a prescribed pressure on the inner cylinder and a prescribed mean axial flow rate is imposed. The outlet velocity field is forced to be fully developed, i.e. $\partial \mathbf{v}/\partial z = 0$. The computations begin with initial velocity and pressure fields of zero and are integrated in time until steady state is reached. We then evaluate the transmembrane pressure and mean axial flow rate at $z = 0$, and use these values for P_{tm} and $\overline{W}$, respectively, to calculate the corresponding analytical solution (3.1) for $-30 \leqslant z \leqslant 30$. For all simulations, the Reynolds number is set to $Re = 50$ to ensure subcritical flow. We verify mesh independence from the decay of the spectral coefficients, and use 50 and 100 Chebyshev polynomials in the r and z directions, respectively.
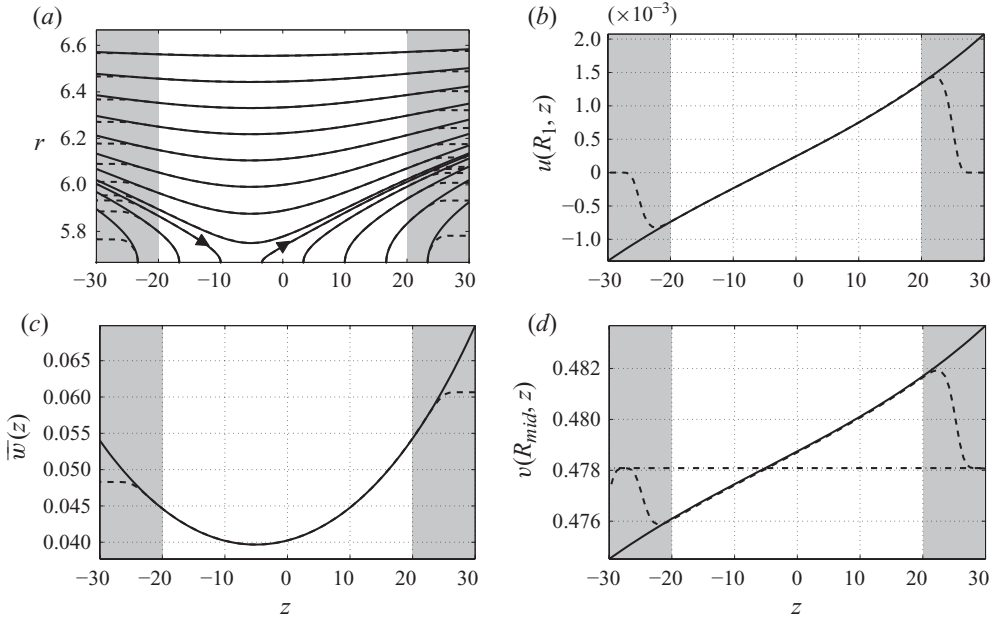
FIGURE 2. Comparison of the asymptotic expansion (3.1) (solid lines) with a direct numerical simulation (dashed lines) of CFR for $\eta = 0.85$, $\sigma = 10^{-4}$, $Re = 50$, $\overline{W} = 0.04025$, $P_{tm} = -0.04886$, $U_{tm} = 2.443 \times 10^{-4}$. The buffer regions have been shaded grey. (*a*) Comparison of streamlines in the r–z plane neglecting the azimuthal velocity. (*b*) Comparison of the axial variation of the transmembrane velocity, $u(R_1, z)$. (*c*) Comparison of the axial variation of mean axial velocity, $\overline{w}(z)$. (*d*) Comparison of the axial variation of the azimuthal velocity at mid-gap $v(R_{mid}, z)$ with $R_{mid} = (R_1 + R_2)/2$. The dash-dotted line depicts the zero-order analytical solution $v_0(R_{mid})$ in (3.1*b*).

Figure 2 illustrates the analytical and numerical results for CFR characterized by $\sigma = 10^{-4}$, $\overline{W} = 0.04025$, $P_{tm} = -0.04886$, $U_{tm} = -\sigma Re P_{tm} = 2.443 \times 10^{-4}$. The non-dimensional permeability, σ, has been set four orders of magnitude larger than typical values to stress that agreement between the analytical and numerical solutions is conserved well beyond usual values for σ. The agreement in figure 2 is very satisfying in the region of interest, $-20 \leqslant z \leqslant 20$, deviating only outside this region in the buffer regions where such deviation is naturally expected due to the function $b(z)$ which modifies the permeability of the numerical solution. The transmembrane flow in figure 2(*b*) reverses from suction in the upstream portion to injection in the downstream portion as the pressure in the annulus decreases in the z direction. Accordingly, the mean axial velocity in figure 2(*c*) decreases with streamwise position for $z < z_{CFR}$, but increases for $z > z_{CFR}$. The numerical simulation yields $z_{CFR} = -5.095$, while (3.2) predicts $z_{CFR} = -5.108$, a relative error of 0.25 %. In the region $-20 \leqslant z \leqslant 20$, the analytical result for $\overline{w}(z)$ is always within 0.1 % of the numerical result. Figure 2(*d*) compares the numerical result for the axial variation of the azimuthal velocity at mid-gap, $R_{mid} = (R_1 + R_2)/2$, with the analytical results v_0 and $v_0 + \epsilon^2 v_2$. In the region $-20 \leqslant z \leqslant 20$, the leading order solution v_0 remains within 0.8 % of the numerical solution. The correction for a permeable cylinder, $v_0 + \epsilon^2 v_2$, improves the agreement to within 0.015 % and demonstrates that suction pulls low-azimuthal-momentum fluid radially inward, while injection pushes high-azimuthal-momentum fluid outward.
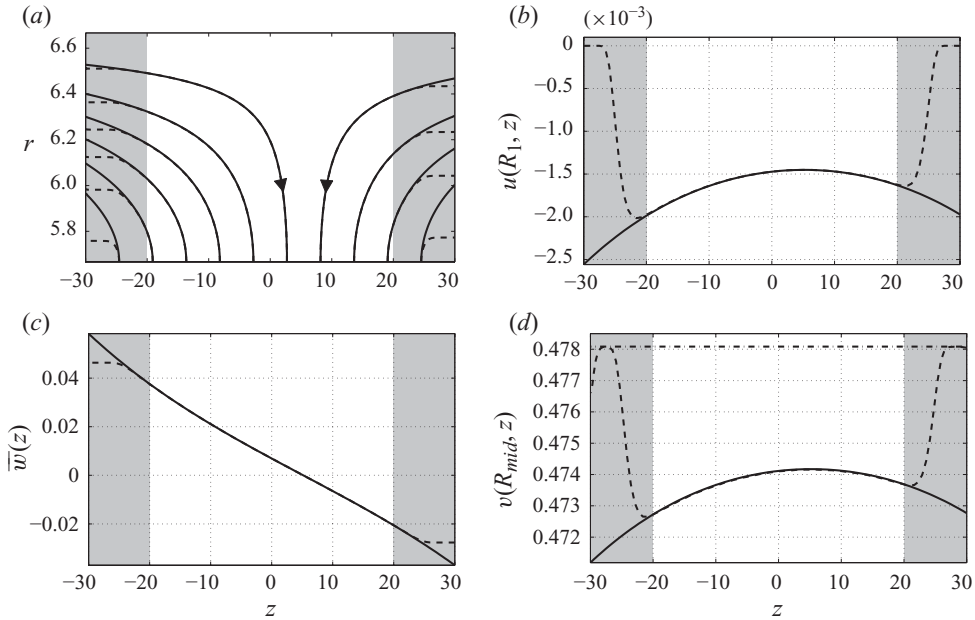
FIGURE 3. Comparison of the asymptotic expansion (3.1) (solid lines) with a direct numerical simulation (dashed lines) of AFE for $\eta = 0.85$, $\sigma = 10^{-4}$, $Re = 50$, $\overline{W} = 6.929 \times 10^{-3}$, $P_{tm} = 0.2945$, $U_{tm} = -1.473 \times 10^{-3}$. (a)–(d) Illustration of the same quantities as in figure 2 using the same conventions.

Figure 3 illustrates AFE for the parameters $\sigma = 10^{-4}$, $\overline{W} = 6.929 \times 10^{-3}$, $P_{tm} = 0.2945$, $U_{tm} = -1.473 \times 10^{-3}$. Fluid enters the system from both ends of the annulus, as is evident from the streamlines in figure 3(a). The mean axial velocity (see figure 3c) vanishes at z_{AFE} where the transmembrane suction (see figure 3b) is minimized. The numerical simulation yields $z_{AFE} = 5.172$, while (3.2) predicts $z_{AFE} = 5.170$. The theory again matches the numerical simulation quite well, and the errors for $\overline{w}(z)$ and $v_0 + \epsilon^2 v_2$ are on the same order as those for the case of CFR.

The agreement between the numerical and analytical results improves as σ tends to zero, and deteriorates as σ increases. Figures 4(a) and 4(b) illustrate the analytical and numerical results for the transmembrane velocity in high-permeability systems exhibiting CFR for $\sigma = 3 \times 10^{-3}$ and AFE for $\sigma = 0.01$, respectively. Both cases display a discrepancy between the analytical and numerical results that increases with axial distance from $z = 0$. This is likely due to two compounding factors. First, the higher order terms, which are neglected in (3.1), become more important as the permeability increases. Second, the exponential behaviour as $z \rightarrow \pm\infty$ is more pronounced in figure 4 than in figures 2 and 3 due to the large permeabilities. Thus, the systems in figure 4 extend outside the region in which variations in the axial direction are small compared to those in the radial direction. Furthermore, because z_{CFR} and z_{AFE} occur upstream of $z = 0$, the exponential behaviour and associated discrepancy are greater on the downstream end of the systems.

We have successfully devised a formulation for Couette–Poiseuille flow with pressure-dependent suction or injection at the inner cylinder. The analytical solution accurately captures the complete velocity and pressure fields, and permits the calculation of z_{CFR} and z_{AFE}, which are important design features for a practical
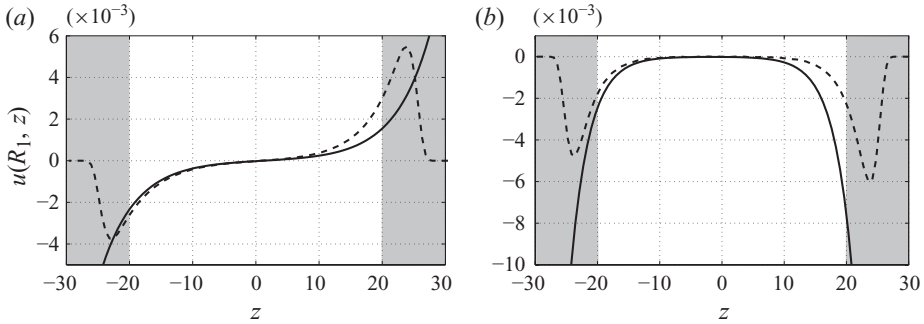
FIGURE 4. Results for high permeabilities showing the discrepancy at large $|z|$ between the numerical simulation (dashed lines) and analytical solution (3.1a) (solid lines) for the transmembrane velocity, $u(R_1, z)$, for $\eta = 0.85$ and $Re = 50$. (a) CFR for $\sigma = 3 \times 10^{-3}$, $\overline{W} = 5.106 \times 10^{-4}$, $P_{tm} = -8.859 \times 10^{-5}$, $U_{tm} = 1.329 \times 10^{-5}$. ($b$) AFE for $\sigma = 0.01$, $\overline{W} = -1.854 \times 10^{-5}$, $P_{tm} = 2.629 \times 10^{-5}$, $U_{tm} = -1.315 \times 10^{-5}$.

system. The success of our method suggests a new approach to find analytic solutions to laminar, wall-bounded, shear flows with pressure-dependent suction or injection. These occur in such diverse applications as crossflow filtration, laminar flow control, transpiration cooling and the transport of biological fluids. This study naturally extends to the study of solute boundary layers and their effect on transmembrane flow through the osmotic pressure. Furthermore, building on previous convective/absolute stability analyses (Martinand *et al.* 2009), (3.1) provide a base flow to study centrifugal instabilities in the form of global modes. This allows accurate computation of the critical conditions for the appearance of vortices and their subsequent spatiotemporal evolution.

REFERENCES

BEAVERS, G. S. & JOSEPH, D. D. 1967 Boundary conditions at a naturally permeable wall. *J. Fluid Mech.* **30**, 197–207.

BELFORT, G., PIMBLEY, J. M., GREINER, A. & CHUNG, K. Y. 1993 Diagnosis of membrane fouling using a rotating annular filter. Part 1. Cell culture media. *J. Membr. Sci.* **77**, 1–32.

BERMAN, A. S. 1953 Laminar flows in channels with porous walls. *J. Appl. Phys.* **24**, 1232–1235.

BERMAN, A. S. 1958 Laminar flow in an annulus with porous walls. *J. Appl. Phys.* **29**, 71–75.

DAMAK, K., AYADI, A., ZEGHMATI, B. & SCHMITZ, P. 2004 A new Navier–Stokes and Darcy's law combined model for fluid flow in crossflow filtration tubular membranes. *Desalination* **161**, 67–77.

GALOWIN, L. S., FLETCHER, L. S. & DESANTIS, M. J. 1974 Investigation of laminar flow in a porous pipe with variable wall suction. *AIAA J.* **12**, 1585–1589.

HALDENWANG, P. 2007 Laminar flow in a two-dimensional plane channel with local pressure-dependent crossflow. *J. Fluid Mech.* **593**, 463–473.

JAFFRIN, M. Y. 2008 Dynamic shear-enhanced membrane filtration: a review of rotating disks, rotating membranes and vibrating systems. *J. Membr. Sci.* **324**, 7–25.

MARQUES, F., SANCHEZ, J. & WEIDMAN, P. D. 1998 Generalized Couette–Poiseuille flow with boundary mass transfer. *J. Fluid Mech.* **374**, 221–249.

MARTINAND, D., SERRE, E. & LUEPTOW, R. M. 2009 Absolute and convective instability of cylindrical Couette flow with axial and radial flows. *Phys. Fluids* **21**, 104102.

MIN, K. & LUEPTOW, R. M. 1994 Circular Couette flow with pressure-driven axial flow and a porous inner cylinder. *Exp. Fluids* **17**, 190–197.

MOREL, J., LAVAN, Z. & BERNSTEIN, B. 1977 Flow through rotating porous annuli. *Phys. Fluids* **20**, 726–733.

REGIRER, S. A. 1960 On the approximate theory of the flow of a viscous incompressible liquid in a tube with permeable walls. *Sov. Phys. Tech. Phys.* **5**, 602–605.

SERRE, E. & PULICANI, J. P. 2001 A three-dimensional pseudospectral method for rotating flows in a cylinder. *Comput. Fluids* **30**, 491–519.

TAYLOR, G. I. 1956 Fluid flow in regions bounded by porous surfaces. *Proc. R. Soc. Lond.* A **234**, 456–475.

YUAN, S. W. & FINKELSTEIN, A. B. 1956 Laminar pipe flow with injection and suction through a porous wall. *Trans. ASME* **78**, 719–724.